ELSEVIER

Journal of Quantitative Spectroscopy & Radiative Transfer 101 (2006) 179–190

Journal of Quantitative Spectroscopy & Radiative Transfer

www.elsevier.com/locate/jqsrt

Understanding the polarization signal of spherical particles for microwave limb radiances

C. Teichmann[a,*,1], S.A. Buehler[a], C. Emde[b]

[a]*Institute of Environmental Physics, University of Bremen, Otto-Hahn-Allee 1, D-28359 Bremen, Germany*
[b]*Deutsches Zentrum für Luft- und Raumfahrt (DLR) Institut für Physik der Atmosphäre, Oberpfaffenhofen, D-82234 Wessling, Germany*

Received 25 March 2005; received in revised form 6 March 2006; accepted 6 March 2006

Abstract

This paper presents a simple conceptual model to explain that even spherical scatterers lead to a polarization difference signal for microwave limb radiances. The conceptual model relates the polarization difference measured by a limb-looking sensor situated inside a cloud with the anisotropy of the radiation. In the simulations, it was assumed that the cloud consists of spherical ice particles with a radius of 68.5 μm which were situated between 10.6 and 12.3 km altitude. The frequencies 318 and 500 GHz were considered.

The results of the conceptual model were compared to the results of the fully polarized scattering model ARTS-1-1. The comparison showed a good qualitative agreement. The polarization difference decreases inside the cloud with increasing height and changes sign. This behavior can be related to a different amount of radiation coming from the atmosphere above and below the cloud, compared to the amount of radiation coming from the sides. The sign of polarization difference of the scattered radiation is opposite for these two radiation sources.

PACS: 42.68.Wt; 42.68.Mj; 41.20.Jb; 84.40.−x

Keywords: Radiative transfer; Microwave remote sensing; Scattering; Cirrus clouds; Limb observations; Polarization difference

1. Introduction

Cirrus clouds play an important role in the Earth's climate system. They permanently cover about 30% of the Earth's surface [1] and influence the Earth–atmosphere radiation balance in such a way that they reflect or transmit solar radiation, but absorb infrared radiation.

Unfortunately, our understanding of the influence of cirrus clouds on climate is limited. The estimated values of the temperature increase given in the IPCC report [2] vary from 1.5 to 4.5 K for a doubling of the CO_2-content. A major reason for this large uncertainty is the limited understanding of clouds and their role in climate.

*Corresponding author.
E-mail address: teichmann@dkrz.de (C. Teichmann).
[1]Now at Max-Planck-Institute for Meteorology, Bundesstrasse 53, 20146 Hamburg, Germany

0022-4073/$ - see front matter © 2006 Elsevier Ltd. All rights reserved.
doi:10.1016/j.jqsrt.2006.03.001

To improve the understanding of clouds, it is necessary to develop numerical models for analysis and retrieval of cloud properties. The retrieval of clouds is important to obtain a global coverage of the properties of cloud particles and ice water content (IWC). Evans and Stephens [3] suggested to use the polarization signal of microwave radiation to help to obtain properties like effective radius and shape of cloud constituents as well as the type of their size distributions.

The analysis of clouds and radiative transfer inside clouds is important to obtain a better understanding of the origin of the polarization difference signal and the relation to the properties of clouds and atmosphere.

Liu and Simmer [4] investigated the polarization signal in down-looking geometry and found that the origin of polarization in clouds with spherical particles can be understood as a combined effect of the anisotropic phase matrix together with varying radiation in the vicinity of the particles. Czekala [5] extended the explanation to non-spherical particles. Miao et al. [6] showed that there is a resonance feature of the polarization difference for ice particles at a certain range of particle size. Prigent et al. [7] showed for the case of 85 GHz that polarized scattering signatures cannot be neglected when generating rain retrieval schemes using scattering properties of the hydrometeor layers.

This paper focuses on the anisotropic radiation field as origin of the polarization difference in limb geometry (looking angle $\gamma \approx 90^{\circ}$) for spherical ice particles. The simplest approach of mono-disperse distribution for the particle size was chosen to explain the polarization difference.

As a reference model for the explanation of polarization difference at limb, the ARTS-1-1-862 model [8] was chosen. There are several polarized plane parallel radiative transfer models [9–14], but ARTS-1-1 is the only polarized model in spherical geometry.

As an example, the polarization difference field in Rayleigh–Jeans brightness temperature (BT) is plotted in Fig. 1 for 500 GHz and ice particles with a radius of 68.5 μm.

One sees that there are positive and negative polarization differences of different magnitudes, depending on height inside the cloud and on the looking angle.

Inside the cloud there is a negative polarization signal for up-looking directions and a positive polarization signal for down-looking directions. Below the cloud only a positive polarization signal for up-looking angles just below 90° zenith angle can be observed. A sensor above the cloud looking in limb geometry will see a positive or negative polarization signal depending on the exact looking angle.

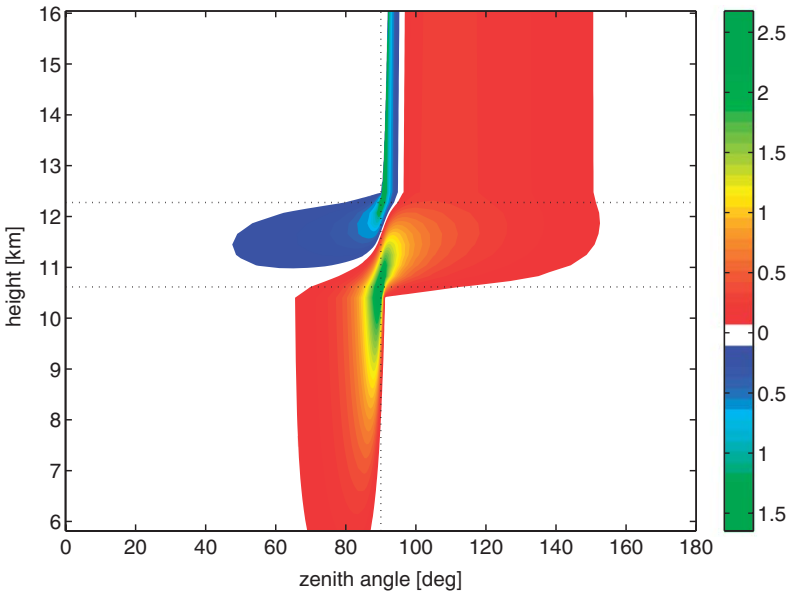

Fig. 1. Polarization difference field for 500 GHz. The polarization difference Q in BT is plotted versus the height in the cloud on the y-axis and the zenith looking angle on the x-axis. The dotted horizontal lines represent the limits of the cloud. Zenith angles below 90° correspond to up-looking and angles above 90° correspond to down-looking geometry, respectively.

In this paper, a simple conceptual model is developed to relate the polarization difference at limb (dotted vertical line in Fig. 1) to the changing amount of radiation coming from different directions in the atmosphere.

The purpose of the conceptual model is not to be used quantitatively, but to provide physical insight into the origin of the polarization signal.

2. Simulation setup

2.1. Definitions

The Stokes vector $\vec{I}$ is defined in terms of the horizontal and vertical component of an electromagnetic wave, E_h and E_v, respectively,

$$\vec{I} = \begin{pmatrix} I \\ Q \\ U \\ V \end{pmatrix} = \frac{1}{2}\sqrt{\frac{\varepsilon}{\mu}} \begin{pmatrix} E_\mathrm{v}E_\mathrm{v}^* & + & E_\mathrm{h}E_\mathrm{h}^* \\ E_\mathrm{v}E_\mathrm{v}^* & - & E_\mathrm{h}E_\mathrm{h}^* \\ -E_\mathrm{v}E_\mathrm{h}^* & - & E_\mathrm{h}E_\mathrm{v}^* \\ \mathrm{i}(E_\mathrm{h}E_\mathrm{v}^* & - & E_\mathrm{v}E_\mathrm{h}^*) \end{pmatrix}, \tag{1}$$

where ε is the permittivity and μ the permeability of the medium in which the electromagnetic wave propagates.

The elements I, Q, U and V of the Stokes vector (often denoted as Stokes parameters) are real values and have the dimension of mono-chromatic energy flux.

In our case of an azimuthally symmetric radiation field and spherical particles, the third and fourth Stokes parameters (U and V) are identically equal to zero. The first two components of the Stokes vector, I and Q, can be related to the vertically polarized and the horizontally polarized part of the radiation (denoted as I_v and I_h, respectively):

$$I = I_\mathrm{v} + I_\mathrm{h}, \tag{2}$$

$$Q = I_\mathrm{v} - I_\mathrm{h}. \tag{3}$$

Here, I is the intensity of the radiation and Q the polarization difference.

In the following, the Stokes vector of the incident radiation and the Stokes vector of the scattered radiation are denoted as $\vec{I}'$ and $\vec{I}$, respectively.

The radiation in the atmosphere for spherical particles can be calculated using the radiative transfer equation (RTE)

$$\frac{\mathrm{d}\vec{I}(\theta,\phi)}{\mathrm{d}s} = -(nC_\mathrm{ext} + \alpha^\mathrm{g})\vec{I} + n\int_{4\pi} \hat{Z}(\theta,\phi,\theta',\phi')\vec{I}'(\theta',\phi')\,\mathrm{d}\omega' + \vec{a}, \tag{4}$$

where $\mathrm{d}s$ is the differential path length along the propagation path of the radiation. The extinction cross section of the particles, which includes absorption as well as extinction due to scattering, is denoted as C_ext, the particle number density as n and the gas absorption coefficient as α^g. The matrix $\hat{Z}(\theta,\phi,\theta',\phi')$ is the phase matrix of the scattering particles, which depends on scattered and incident directions; θ and ϕ are zenith and azimuth angle, respectively. The differential solid angle element is defined as $\mathrm{d}\omega = \sin\theta\,\mathrm{d}\theta\,\mathrm{d}\phi$. The vector $\vec{a}$ represents the emission of particles and atmosphere. For oriented non-spherical particles the extinction cross section C_ext would have to be replaced by a matrix.

The total extinction coefficient, which includes particle extinction as well as gas absorption, can be defined as

$$K_\mathrm{ext} = nC_\mathrm{ext} + \alpha^\mathrm{g}. \tag{5}$$

For a macroscopically isotropic and symmetric medium, the single scattering properties can be completely described by the scattering matrix

$$\hat{F}(\theta) = \hat{Z}(\theta, \phi = 0, \theta' = 0, \phi' = 0). \tag{6}$$

Our simple test case with spherical particles belongs to this class of medium. For detailed definitions and derivations of scattering and phase matrix refer to Mishchenko et al. [15].

The optical thickness τ is defined as

$$\tau = K_{\text{ext}} s. \tag{7}$$

In a layer of constant gas absorption, K_{ext} can be assumed as constant.

2.2. The atmosphere

The properties and constituents of both atmosphere and cloud were assumed to vary only with altitude (1D atmosphere). This corresponds to a totally cloud-covered Earth, which is of course unrealistic. Nevertheless, the scenario is not too different from a widely extended cloud and permits to investigate the upper limit of the polarization effect.

The included species are H_2O, O_3, N_2 and O_2 with profiles taken from the FASCOD [16] midlatitude summer scenarios. The temperature profile is also taken from the FASCOD-scenario. Gas absorption is calculated using the ARTS-1-0 scalar model [17] based on the HITRAN [18] molecular spectroscopical database.

2.3. The cloud

The calculations were performed for a 1D cloud with an extent from 10.6 to 12.3 km altitude and an ice mass content (IMC) of $0.05\,\text{g/m}^3$. At the upper and lower limit of the cloud the IMC decreases linearly to zero. The choice of a rather high and strong cloud was motivated by the aim to investigate a possible maximum of the polarization signal. The aim of a better understanding of the polarization inside the cloud justifies the assumption of spherical ice particles and a mono-size-distribution. The radius of the ice particles was fixed at 68.5 μm.

2.4. Observation setup

Since no specific sensor pattern was used, all quantities shown in this article can be thought of being measured by an ideal sensor. It can be situated anywhere in the atmosphere and look in any direction.

Calculations were done for two frequencies: 318 and 500 GHz. The choice was motivated by the absorption of the atmosphere and by the different single scattering properties at both frequencies. For 318 GHz gas absorption is small, whereas for 500 GHz gas absorption is rather high. At an altitude of 11.4 km, the gas absorption coefficient a for 318 and 500 GHz is $a = 2.2 \times 10^{-6}\,1/\text{m}$ and $3.2 \times 10^{-6}\,1/\text{m}$, respectively.

For the assumed IMC and particle size, and a temperature of 226 K, the scattering cross section for 318 GHz is $C_{\text{sca}} = 3.2 \times 10^{-10}\,\text{m}^2$, whereas for 500 GHz, $C_{\text{sca}} = 20.3 \times 10^{-10}\,\text{m}^2$. The single scattering albedo for the particles, $\overline{\omega}$, is defined as the ratio of scattering cross section (C_{sca}) and extinction cross section (C_{ext}):

$$\overline{\omega} = \frac{C_{\text{sca}}}{C_{\text{ext}}}. \tag{8}$$

In the setup, the single scattering albedo is rather high for both frequencies—318 GHz ($\overline{\omega} = 0.86$) and 500 GHz ($\overline{\omega} = 0.93$). This means that interaction of particles and radiation is dominated by scattering rather than by absorption.

The single scattering albedo for the atmosphere including gas absorption $\overline{\omega}'$ is defined as the ratio of scattering coefficient (nC_{sca}) and the total extinction coefficient (K_{ext}):

$$\overline{\omega}' = \frac{nC_{\text{sca}}}{K_{\text{ext}}}. \tag{9}$$

Also the interaction between radiation and atmosphere, including gas absorption and particle interaction, is dominated by scattering of the particles: the single scattering albedo for the atmosphere at an altitude of 11.4 km is $\overline{\omega}' = 0.76$ and 0.90 for 318 and 500 GHz, respectively.

The phase matrix depends strongly on the ratio between particle size and wavelength. To distinguish between the different scattering regimes, we define the Mie-parameter

$$m = \frac{2\pi d}{\lambda}, \tag{10}$$

where d is the diameter of the scattering particle and λ the wavelength of the scattered radiation. For the setup used in this paper, the Mie-parameter is $m = 0.9$ for 318 GHz and $m = 1.4$ for 500 GHz. Therefore, the calculations are performed in the Mie-regime.

2.5. Reference RT model

The calculations presented in this article were performed with the ARTS-1-1 model, which includes a polarized discrete ordinate scattering algorithm using spherical geometry. The scattering calculations are performed inside a predefined volume named "cloudbox". Inside this volume, the RTE is solved by the discrete ordinate iterative (DOIT) method [19]. Obviously, the cloudbox should surround the region where scattering particles forming a cloud are situated. Outside the cloudbox, clear-sky radiative transfer is performed.

The radiation field inside the cloudbox is represented by a set of Stokes vectors. They are situated on grid points of three predefined grids: pressure, longitude and latitude. As in the 1D case, the radiation depends neither on longitude nor on latitude, only one set of Stokes vectors for each pressure level needs to be stored.

Stokes vectors at a certain altitude only depend on the vertical looking direction, denoted as zenith angle. Due to the anisotropy of the radiation field and the strong gradient in limb direction, an optimized grid for the calculation of the scattering integral is needed. The density of grid points is highest around a zenith angle of 90°.

The cloudbox extends from 6 to 16 km. The single scattering properties of the ice particles were calculated using PyARTS [20] which includes the T-matrix code from Mishchenko and Travis [21]. The refractive index of ice, which is used by the T-matrix code, was computed using a code developed by Warren [22].

3. Simulation results

In Fig. 2, the polarization difference Q, calculated by the reference model, is plotted against the height in the atmosphere for a constant zenith angle of $\gamma = 90°$. This corresponds to the vertical dotted line in Fig. 1.

Starting near the ground, an increase of Q can be observed below the cloud from 0 K BT to about 2.7 K BT with increasing height for 500 GHz. The maximum value for 318 GHz is about 0.5 K BT. Inside the cloud Q decreases to negative values for both frequencies. The altitude where Q is zero differs for both frequencies: for 318 GHz Q is zero at 11.1 km altitude and for 500 GHz at 11.7 km altitude. Q reaches a minimum at about 12.3 km altitude inside the cloud in both cases. For 318 GHz the value of the minimum is about −1 K BT and for 500 GHz about −1.7 K BT. Above the cloud Q is zero.

4. Interpretation with a simple conceptual model

With the simple conceptual model, the origin of the polarization difference signal can be explained for this special case of spherical particles and a looking angle γ of 90°.

From Eqs. (4) and (7) the polarization difference of the scattered radiation can be derived as

$$\frac{\mathrm{d}Q}{\mathrm{d}\tau} = -Q + \frac{n}{K_{\mathrm{ext}}} \int_{4\pi} (Z_{21} I' + Z_{22} Q') \, \mathrm{d}\omega'. \tag{11}$$

In the simple conceptual model, the integral in Eq. (11) is assumed to be constant inside a layer. As the first term in the integral is several orders of magnitude larger than the second, Q is determined by the incoming

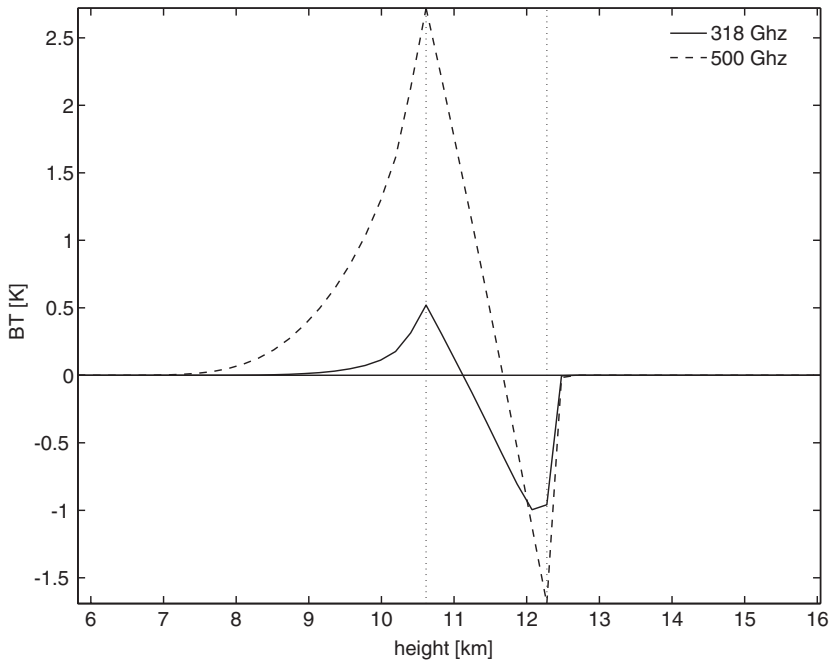

Fig. 2. Q as a function of height. The polarization difference Q in BT is plotted against the height in the atmosphere. The different lines correspond to the frequencies 318 (solid line) and 500 GHz (dashed line). The dotted vertical lines represent the cloud.

radiation I' and the component Z_{21} of the phase matrix:

$$\frac{\mathrm{d}Q}{\mathrm{d}\tau} \approx -Q + \frac{n}{K_{\mathrm{ext}}} \int_{4\pi} Z_{21} I' \mathrm{d}\omega'. \tag{12}$$

Solving Eq. (12) and considering the limit of high opacity $\tau \to \infty$ leads to

$$Q \approx \frac{n}{K_{\mathrm{ext}}} \int_{4\pi} Z_{21} I' \, \mathrm{d}\omega'. \tag{13}$$

For the special case $\phi = \theta' = \phi' = 0$, the scattering matrix is equal to the phase matrix (cf. Eq. (6)). In Fig. 3, the scattering matrix component F_{21} is plotted versus the scattering angle. It is part of the single scattering properties of the particles. The maximum absolute value of F_{21} is at a scattering angle Θ of approximately 90°. Eq. (13) shows that also the absolute value of Q has a maximum around 90° scattering angle for a fixed incident intensity I'.

For simplicity, fully polarized radiation is assumed for scattering angles $\Theta \in (45°, 135°)$ in the simple conceptual model. While this is strictly true only in the Rayleigh regime at a scattering angle of $\Theta = 90°$, it is at least approximately true also for $\Theta \in (45°, 135°)$ in the Mie regime. Additionally, unpolarized radiation is assumed for scattering angles $\Theta \notin (45°, 135°)$. This simplification is equal to the following definition for the phase matrix dependency on the scattering angle Θ:

$$Z_{21}(\Theta) = \begin{cases} F_{21}(\Theta = 90°): & \Theta \in (45°, 135°), \\ 0: & \Theta \notin (45°, 135°). \end{cases} \tag{14}$$

Furthermore, the electric field vector of the scattered radiation is assumed to be perpendicular to the scattering plane. This leads to two main contributions to the Q signal at a point P with $\gamma = 90°$ looking angle: radiation coming from above (I_{above}) and below (I_{below}) the cloud on the one hand and from both sides (I_{sides}) on the other hand (cf. Fig. 4). As a 1D atmosphere is used, P is only a function of altitude: $P = P(h)$.

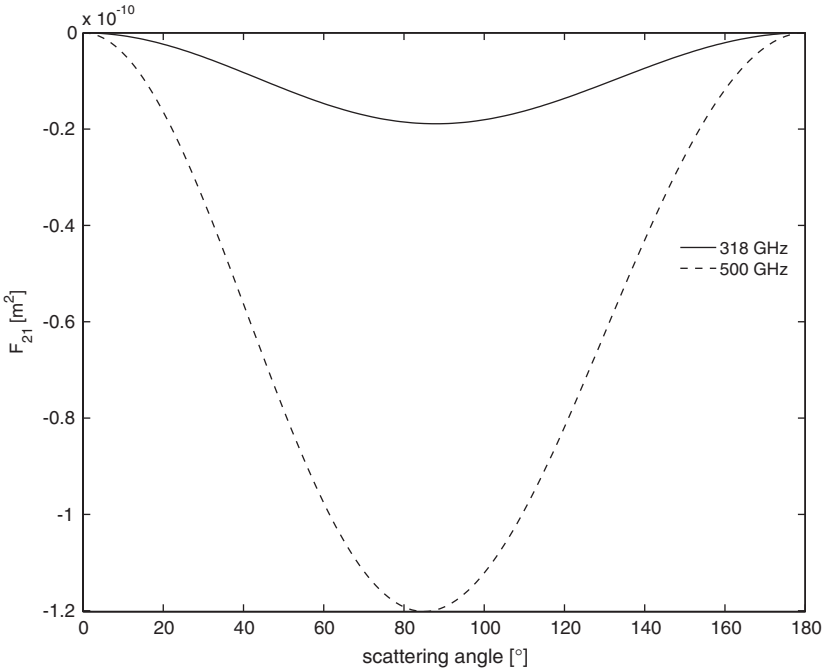

Fig. 3. Scattering matrix component F_{21}. The scattering matrix component F_{21} is plotted versus the scattering angle. The frequencies 318 and 500 GHz are represented by solid and dashed lines, respectively.

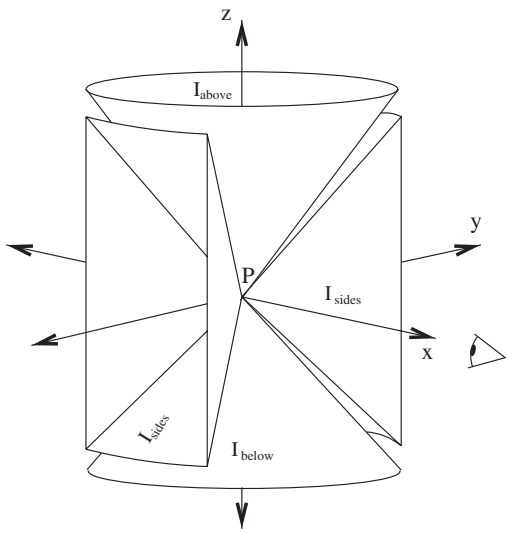

Fig. 4. Solid angles of incoming radiation. Inside the cloud, the considered contributions to scattering at point P on the origin are: I_{sides} (corresponding to positive and negative y-axis), I_{below} (corresponding to negative z-axis) and I_{above} (corresponding to positive z-axis). The observer is looking in negative x-direction.

Radiation coming from above the cloud and scattered inside the cloud into the line of sight, at a scattering angle $\Theta \in (45^\circ, 135^\circ)$, leads to horizontally polarized scattered radiation. It is therefore a negative contribution to Q (cf. Eq. (3)). The radiation coming from below the cloud has the same effect. Scattered radiation from the sides (also at $\Theta \in (45^\circ, 135^\circ)$) is vertically polarized. This leads to a positive contribution to Q.

The contributions were calculated using the ARTS-1-1 model and by integrating the incident radiation I' over a solid angle $\Omega = 1.84\,Sr$ for each direction:

$$I_{\text{above}} = \int_0^{45} \sin\theta' \mathrm{d}\theta' \int_0^{360} \mathrm{d}\phi' I'(\theta', \phi'), \tag{15}$$

$$I_{\text{below}} = \int_{135}^{180} \sin\theta' \mathrm{d}\theta' \int_0^{360} \mathrm{d}\phi' I'(\theta', \phi'), \tag{16}$$

$$I_{\text{sides}} = \int_{45}^{135} \sin\theta' \mathrm{d}\theta' \int_{52.7}^{127.2} \mathrm{d}\phi' I'(\theta', \phi') + \int_{45}^{135} \sin\theta' \mathrm{d}\theta' \int_{232.8}^{307.3} \mathrm{d}\phi' I'(\theta', \phi'). \tag{17}$$

The solid angle Ω corresponds to a cone with an opening angle of 45° for I_{above} and I_{below}. This means that $\phi \in (0^\circ, 360^\circ)$ and $\theta \in (0^\circ, 45^\circ)$ for I_{above} and $\phi \in (0^\circ, 360^\circ)$ and $\theta \in (135^\circ, 180^\circ)$ for I_{below}. For the case of I_{sides}, the spherical sector is defined as $\phi \in (52.7^\circ, 127.2^\circ)$ or $\phi \in (232.8^\circ, 307.3^\circ)$ and $\theta \in (45^\circ, 135^\circ)$. These bounds were chosen such that each of the four integration areas covers an equal solid angle interval. They are illustrated in Fig. 4.

With the sign of the contributions deduced from the physical considerations and Eqs. (15)–(17), the polarization in the simple model can be calculated from Eqs. (13) and (14) as

$$Q = \frac{n|Z_{21}|}{K_{\text{ext}}}(I_{\text{sides}} - (I_{\text{above}} + I_{\text{below}})). \tag{18}$$

The averaged integrated incoming radiation components are defined as

$$\begin{aligned} \bar{I}_{\text{above}} &= \frac{I_{\text{above}}}{\Omega}, \\ \bar{I}_{\text{below}} &= \frac{I_{\text{below}}}{\Omega}, \\ \bar{I}_{\text{sides}} &= \frac{I_{\text{sides}}}{2\Omega}. \end{aligned} \tag{19}$$

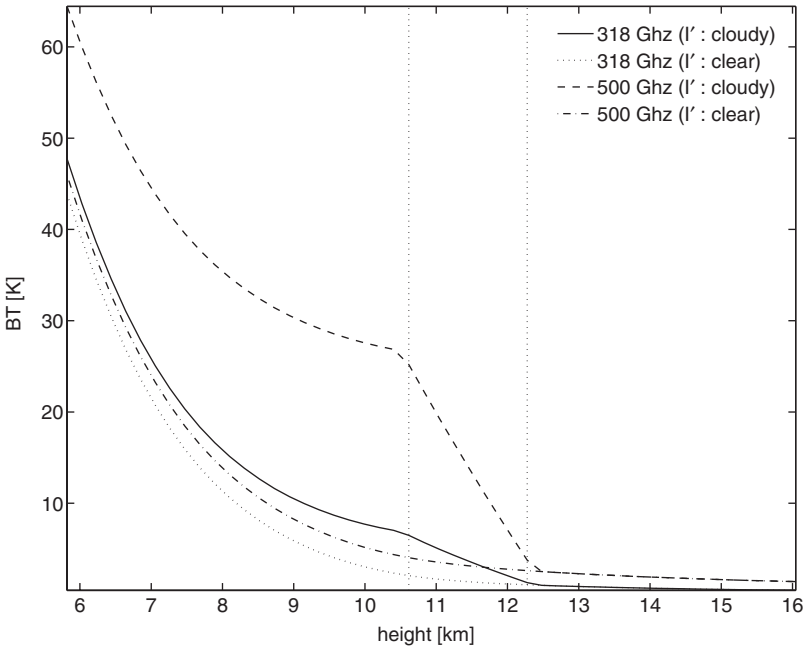

Fig. 5. Radiation coming from above. The averaged integrated incident radiation from above in BT is plotted versus the height in the atmosphere from which it is observed. The solid and the dashed lines represent the 318 and 500 GHz case, respectively. The dotted and dash dotted lines represent the clear-sky cases for 318 and 500 GHz, respectively.

In Fig. 5, the averaged incoming radiation from above $\bar{I}_{\text{above}}$ is plotted against the height at which it is observed. The cloudy cases are calculated using the cloudy radiance field, and the clear-sky cases are calculated using the clear-sky radiance field from the ARTS-1-1 model as incoming radiation in Eqs. (15)–(17). For both frequencies, an enhancement of BT can be observed for the scattering cases below the cloud due to the radiation scattered into the line of sight. The difference to the clear-sky case below the cloud is smaller for lower altitudes. In this case, the distance to the cloud is bigger and the gas absorption is higher. Therefore, the influence of the cloud is smaller. For 500 GHz, more radiation is scattered into the line of sight than for 318 GHz. This can be explained by a higher single scattering albedo for the atmosphere $\overline{\omega}'$ at 500 GHz (cf. Section 2.4). Inside the cloud the enhancement decreases and reaches zero at the top of the cloud.

Fig. 6 shows the averaged integrated incident radiation coming from below $\bar{I}_{\text{below}}$. One observes a BT depression relative to the clear-sky case for both frequencies. Inside the cloud up-welling radiation from below is scattered out of the line of sight, whereas below and above the cloud no changes of the difference to the clear-sky case are observable.

The magnitude of the depression is about 4 K BT for 318 GHz and about 18 K BT for 500 GHz.

In Fig. 7, the averaged integrated radiation coming from both sides $\bar{I}_{\text{sides}}$ is plotted against the height in the cloud. Below the cloud, a BT enhancement of up to about 42 K BT can be observed for 500 GHz and up to about 20 K BT for 318 GHz. The enhancement increases with increasing height in the atmosphere as more and more radiation is scattered into the line of sight by the cloud. Inside the cloud the enhancement decreases. With increasing height inside the cloud, the fraction of radiation which is scattered out of the line of sight grows. This leads to a BT depression in the upper third of the cloud. Above the cloud the difference and, therefore, the influence of the cloud stays constant. This is explainable by the small gas absorption above the cloud. The fraction of the cloud inside the viewing-cone of the sensor stays approximately constant.

In Fig. 8, the polarization difference Q, calculated using the simple model, is plotted versus the height in the atmosphere. It is given by Eq. (18).

The main features of the polarization difference (cf. Fig. 2) are reproduced by the simple model inside the cloud: in both calculations—reference model ARTS-1-1 and simple model—Q is bigger for 500 GHz than for

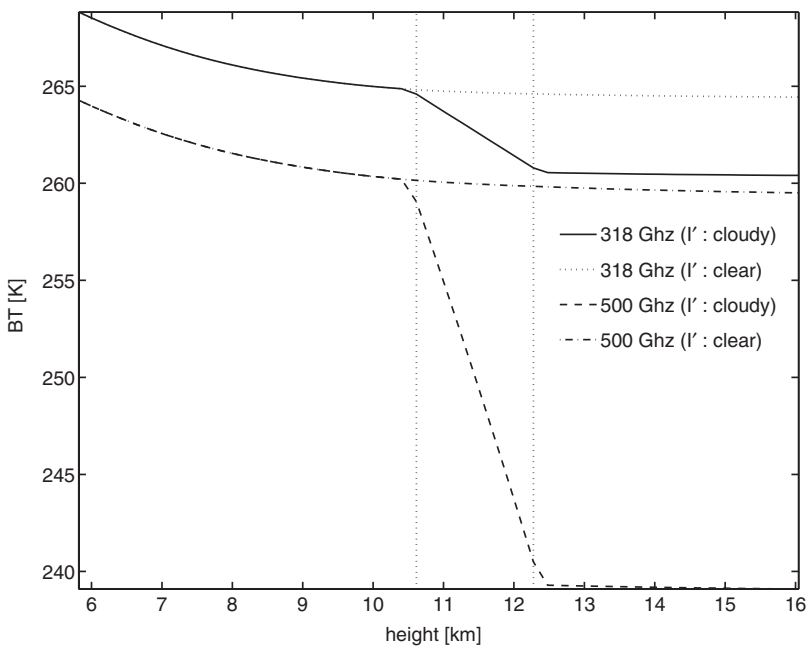

Fig. 6. Radiation coming from below. The averaged integrated incident radiation from below in BT is plotted versus the height in the atmosphere from which it is observed. The solid and the dashed lines represent the 318 and 500 GHz case, respectively. The dotted and dash dotted lines represent the clear-sky cases for 318 and 500 GHz, respectively.

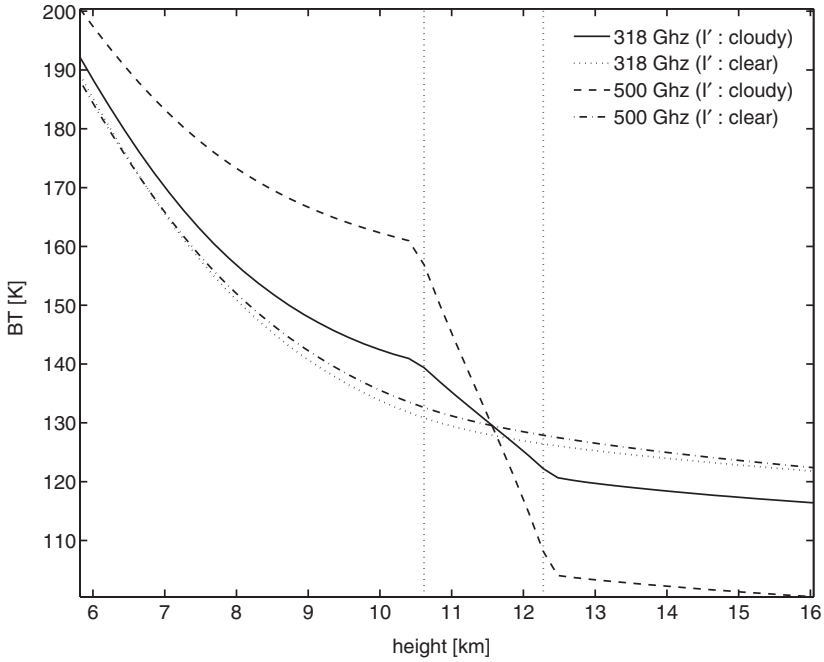

Fig. 7. Radiation coming from the sides. The averaged integrated incident radiation from both sides in BT is plotted against the height in the atmosphere from which it is observed. The solid and the dashed lines represent the 318 and 500 GHz case, respectively. The dotted and dash dotted lines represent the clear-sky cases for 318 and 500 GHz, respectively.

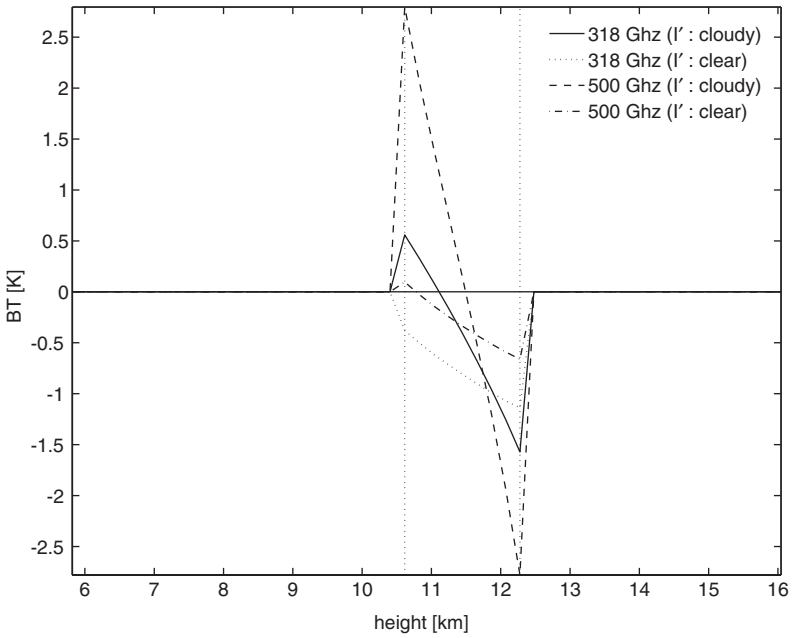

Fig. 8. Q from the simple model. The polarization difference Q in BT, calculated using the simple model, is plotted versus the height in the atmosphere from which it is observed. The solid and the dashed lines represent the 318 and 500 GHz case, respectively. The dotted and dash dotted lines represent the cases for 318 and 500 GHz, where the clear-sky fields are taken as input for the integral in Eq. (18).

318 GHz in the lower and middle part of the cloud, whereas it is smaller in the upper part. At the lower border of the cloud the magnitude of the polarization signal could be reproduced: the BT values for the simple model are 0.04 and 0.08 K BT higher than in the reference model for 318 and 500 GHz, respectively.

The height where Q changes sign is $h_s = 11.1$ km altitude for 318 GHz for the simple and the reference model, whereas there is a difference for 500 GHz: $h_s = 11.7$ km in the reference model and $h_s = 11.5$ km in the simple model.

The minima at the upper border of the cloud in the simple model differ from the minima in the reference model. For 318 GHz the values for simple and reference model are $Q = -1.6$ and -1 K BT, respectively, and for 500 GHz the values for simple and reference model are $Q = -2.8$ BT and -1.7 K BT, respectively.

As the simple model uses a plane parallel geometry, the polarization signal is zero at altitudes below and above the cloud due to the absence of scattering particles. Polarization cannot propagate from one layer into the other. This is not the case for the reference model, where positive polarization difference can be observed below the cloud down to about 8 km altitude for 500 GHz. The polarization difference is generated inside the cloud and propagates to lower layers where it can be observed in limb geometry due to the sphericity of the atmosphere.

It is also possible to calculate the polarization difference using the clear-sky field as input to Eq. (18). The result is plotted in Fig. 8 for 318 GHz (dotted line) and 500 GHz (dash dotted line). A qualitative comparison with the reference model (cf. Fig. 1) shows that the polarization difference is not reproduced with the simple model using clear-sky radiances as input. This means that single scattering cannot be assumed inside the cloud: one has to take into account the multiply scattered radiation in the whole cloud into the line of sight or out of it.

5. Summary and conclusions

The simple conceptual model is able to reproduce the polarization difference. A good quantitative agreement with the reference model was obtained for values at the lower border of the cloud. The deviation of the simple model to the reference model at the upper border of the cloud can be explained: to fulfill the assumption of a high optical depth ($\tau \to \infty$), the assumed line of sight (LOS) has to be longer (and the layer enclosing the considered LOS thicker) above the cloud, than inside the cloud (cf. Eq. (7)). At the cloud top, the LOS leaves the cloud rather quickly due to the spherical geometry. Therefore, the assumption of constant cloud properties inside a plane parallel layer in the simple model is worse at the upper border of the cloud leading to a deviation from the reference model.

The sign-change of Q at a certain cloud altitude at 90° looking angle inside the cloud for spherical ice particles can be explained. The origin of the sign-change of Q is a changing contribution of radiation from above, below and the two sides. The strong decrease of I_{sides} leads to a strong decrease of I_{v} with height. The relatively weak decrease of I_{above} and I_{below} leads to a relatively small decrease of I_{h}. Together with a higher absolute value of I_{sides} at the bottom of the cloud, this explains the positive Q decreasing to negative values inside the cloud.

Further investigations can be done concerning the validity of the simple model for looking directions other than limb and for particles other than spheres.

Acknowledgements

We thank Oliver Lemke for programming assistance and technical support. Furthermore, we thank Michael Mishchenko and Stephan Warren for making available the T-matrix program and the refractive index program, respectively. Thanks to Cory Davis for providing the PyARTS package.

Thanks to the ARTS radiative transfer community, many of whom have indirectly contributed by implementing features to the ARTS model.

This study was funded by the German Federal Ministry of Education and Research (BMBF), within the DLR project SMILES, Grant 50 EE 9815, and within the AFO2000 project UTH-MOS, Grant 07ATC04.

References

[1] Wylie DP, Menzel WP, Woolf HM, Strabala KI. Four years of global cirrus cloud statistics using hirs. J. Climate 1994;7(12):1972–86.
[2] IPCC. Technical summary: A report accepted by working group I of the IPCC but not approved in detail. Technical Report, IPCC; 2001.

[3] Evans KF, Stephens GL. Microwave radiative transfer through clouds composed of realistically shaped ice crystals. part II: Remote sensing of ice clouds. J. Atmos. Sci. 1995;52(11):2058–72.
[4] Liu Q, Simmer C. Polarization and intensity in microwave radiative transfer. Beitr. Phys. Atmos. 1996;69(4):535–45.
[5] Czekala H. Effects of ice particle shape and orientation on polarized microwave radiation for off-nadir problems. Geophys. Res. Lett. 1998;25(10):1669–72.
[6] Miao J, Johnsen K-P, Buehler SA, Kokhanovsky A. The potential of polarization measurements from space at mm and sub-mm wavelengths for determining cirrus cloud parameters. Atmos. Chem. Phys. 2003;3:39–48.
[7] Prigent C, Pardo JR, Mishchenko MI, Rossow WB. Microwave polarized signatures generated within cloud systems: Special sensor microwave imager (SSM/I) observations interpreted with radiative transfer simualtions. J. Geophys. Res. 2001;106(D22):28243–58.
[8] Eriksson P, Buehler SA, Emde C, Sreerekha TR, Melsheimer C, Lemke O. ARTS-1-1 User Guide, University of Bremen; 2004: 308p. regularly updated versions available at ⟨www.sat.uni-bremen.de/arts/⟩.
[9] Gasiewski AJ, Stalin DH. Numerical modeling of passive microwave O_2 observations over precipitation. Radio Sci. 1990; 25(3):217–35.
[10] Evans KF, Stephens GL. A new polarized atmospheric radiative transfer model. JQSRT 1991;46(5):412–23.
[11] Eyre J. A fast radiative transfer model for satellite sounding systems. Technical Report, ECMWF Technical Memo. No. 176; 1991.
[12] Simmer C. Satellitenfernerkundung hydrologischer Parameter der Atmosphäre mit Mikrowellen, 2nd ed. Verlag Dr. Kovac; 1994.
[13] Haferman JL, Smith TF, Krajewski WF. A multi-dimensional discrete-ordinates method for polarised radiative transfer part 1: Validation for randomly oriented axisymmetric particles. JQSRT 1997;58:379–98.
[14] Schulz FM, Stamnes K, Weng F. Vdisort: an improved and generalized discrete ordinate method for polarized (vector) radiative transfer. JQSRT 1999;61(1):105–22.
[15] Mishchenko MI, Travis LD, Lacis AA. Scattering absorption and emission of light by small particles. Cambridge, MA: Cambridge University Press; 2002 ISBN 0-521-78252-X.
[16] Anderson GP, Clough SA, Kneizys FX, Chetwynd JH, Shettle EP. AFGL atmospheric constituent profiles (0–120 km). Technical Report TR-86-0110, AFGL; 1986.
[17] Buehler SA, Eriksson P, Kuhn T, von Engeln A, Verdes C. ARTS, the atmospheric radiative transfer simulator. JQSRT 2005;91(1):65–93.
[18] Rothman LS, Rinsland CP, Goldman A, Massie ST, Edwards DP, Flaud J-M, et al. The HITRAN molecular spectroscopic database and HAWKS (HITRAN atmospheric workstation): 1996 edition. JQSRT 1998;60:665–710.
[19] Emde C, Buehler SA, Davis C, Eriksson P, Sreerekha TR, Teichmann C. A polarized discrete ordinate scattering model for simulations of limb and nadir longwave measurements in 1D/3D spherical atmospheres. J. Geophys. Res. 2004;109(D24).
[20] Davis C. PyARTS, ⟨http://www.met.ed.ac.uk/~cory/PyARTS⟩; 2004.
[21] Mishchenko MI, Travis LD. Capabilities and limitations of a current FORTRAN implementation of the T-matrix method for randomly oriented rotationally symmetric scatterers. JQSRT 1998;60:309–24.
[22] Warren S. Optical constants of ice from the ultraviolet to the microwave. Appl. Opt. 1984;23:1206–25.